Sources and calibration of space point distortions in a TPC

using the example of ALICE

Pascal Becht

Particle Tracking and Identification at High Rates
Master Seminar, WS 2017/18
University of Heidelberg

January 19, 2018

Outline

1. Motivation
2. Static Distortions
   - Langevin Equation
   - RUN 1
3. Dynamic Distortions
   - RUN 2
   - RUN 3 (expectations)
4. Conclusion

General Goals

- Track reconstruction
- Particle identification
  - Momentum p, p_{T}
  - Energy loss dE/dx

$\Rightarrow$ Best possible resolution

As a consequence:

- Distortion calibration better than intrinsic resolution

$\mathcal{O}$ 1 mm (single space point)

$\mathcal{O}$ 200 µm (tracklet)

Figure 1 Distorted (blue) and corrected (red) track [2]

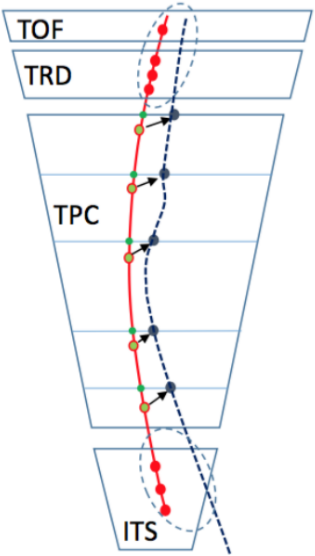

p_T Resolution

Gluckstern formula (for high p_T tracks):

$$\left|\frac{dp_T}{p_T}\right|_{res} = \frac{\sigma_{point}}{eB_0 L^2}\sqrt{\frac{720}{N_{eff}+4}}\, p_T \qquad (1)$$

L: Projected length of the track on the bending plane

$N_{eff} = N_{point}$: # equidistant, uncorrelated measurement points

ALICE TPC: N_{point}=159

No multiple scattering

BUT:

- Distorted space points are strongly correlated

⇒ Need a high(er) space point resolution for a given p_T resolution:

ALICE TPC: $\frac{\sigma_{point}}{\sqrt{N_{point}/3}} = \frac{0.1\,\mathrm{cm}}{\sqrt{159/3}} \approx 150\,\mu\mathrm{m}$

Space Point Correlation

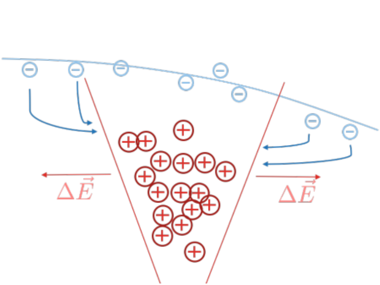

Figure 2 Sketch of space point correlation due to space charge [3]

- $\rho_{\text{ion}} = \langle\rho\rangle + \sigma_\rho$
- σ_ρ : $\mathcal{O} \pm 20\,\%$

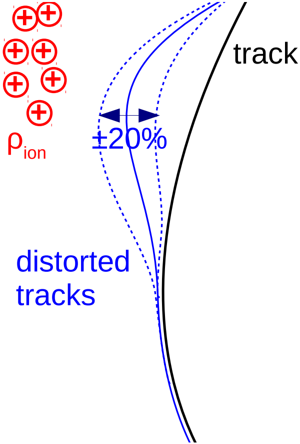

Figure 3 Modified mean trajectory (solid) with fluctuations (dashed)

Precision Requirements

- Correction for distortions down to intrinsic resolution

$\Rightarrow$ Precision criteria:

$$\sigma_{\text{dist}} \leq \frac{\sigma_{\text{cluster}}}{\sqrt{N_{\text{corr}}}} \qquad (2)$$

Example (line charge RUN2):

$\sigma_{\text{cluster}} = 1\,\text{mm}$

$N_{\text{corr}} = \frac{N_{\text{point}}}{N_{\text{eff}}} = 20$

$\Rightarrow \sigma_{\text{dist}} < 225\,\mu\text{m}$

$\Rightarrow$ N_{corr} strongly depends on source of distortion

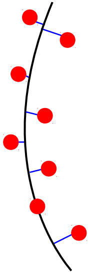

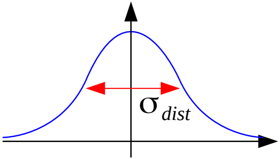

Figure 4 Visualisation of distortion distribution (Cauchy)

Motion of Charged Particles

Langevin equation (effective theory):

$$m\frac{d\vec{u}}{dt} = e\vec{E} + e\left(\vec{u} \times \vec{B}\right) - K\vec{u} \tag{3}$$

Static solution $\frac{d\vec{u}}{dt} = 0$:

$$\vec{u} = \frac{e}{m}\tau|\vec{E}|\frac{1}{1+\omega^2\tau^2}\left(\hat{\vec{E}} + \omega\tau\left(\hat{\vec{E}} \times \hat{\vec{B}}\right) + \omega^2\tau^2\left(\hat{\vec{E}} \cdot \hat{\vec{B}}\right) \cdot \hat{\vec{B}}\right) \tag{4}$$

K: friction parameter

$\tau = m/K$

$\omega = qB/m$

$\omega\tau$: detector specific

ALICE TPC:

$\omega\tau = 0.3$ for e^-

$\omega\tau \approx 0$ for ions

$\Rightarrow$ Ideal case: $\hat{\vec{E}} \parallel \hat{\vec{B}}$, $\hat{\vec{E}} \perp \hat{\vec{S}}$

$(\hat{\vec{E}} \times \hat{\vec{B}} = 0)$

RUN1

2005 – 2013

- Interaction rate: $\mathcal{O}$ 100 Hz (Pb-Pb)
- MWPC readout

Field Cage

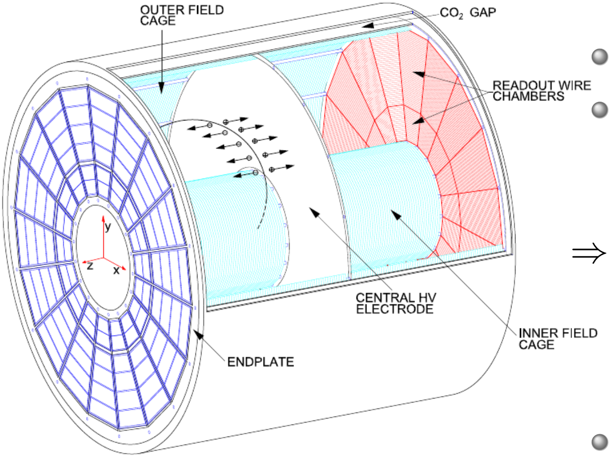

Figure 5 Sketch of the ALICE TPC field cage by D. Vranic [4]

- $\hat{\vec{E}} \parallel \hat{\vec{B}}$, $\hat{\vec{E}} \perp \hat{\vec{S}}$
- Strips with decreasing potential

$\Rightarrow$ Minimise E field inhomogenities due to boundary effects

- Physical models of distortions on next slides

Static Distortions and their Calibration

- E field inhomogenities at the boundary
- Mechanical misalignment of the CE
- Field cage misalignment
- B field inhomogenities
- $E \times B$ twist
- Calibration

E Field Inhomogenities at the Boundary

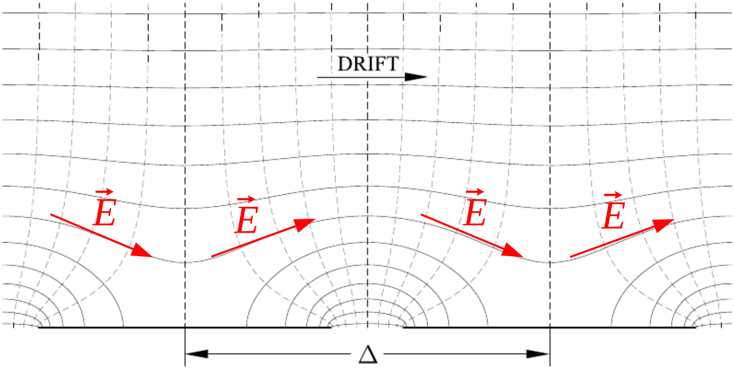

Figure 6 Sketch of the working principle of the field cage by D. Vranic. Remaining inhomogenity depth $\frac{E_r}{E_z} \sim e^{-\frac{d}{\Delta}}$. $\Delta = 270\,\mathrm{mm}$ [4]

Mechanical Misalignment

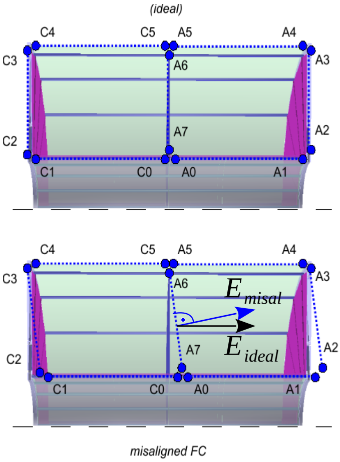

Figure 7 Sketch of a CE misalignment scenario. CE shifted by 1 mm [5]

- Mechanical misalignment $\hat{=}$ E field distortions
- $\mathcal{O}$ 1 mm misalignment $\rightarrow$ $\mathcal{O}$ 1 mm distortion:

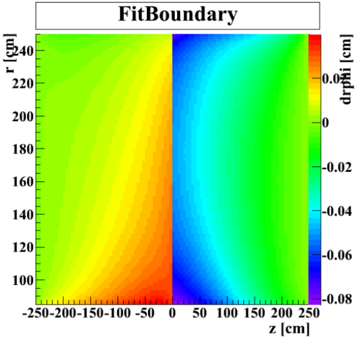

Figure 8 Resulting $dr\phi$ [6]

Field Cage and Rod Misalignment

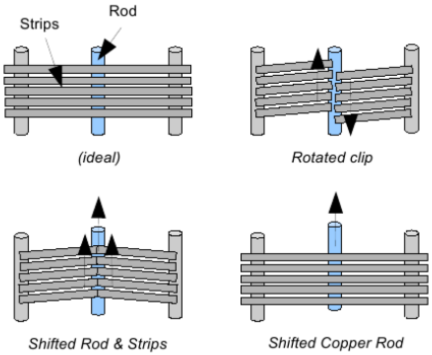

Figure 9 Sketch of different rod and strip misalignment scenarios [5]

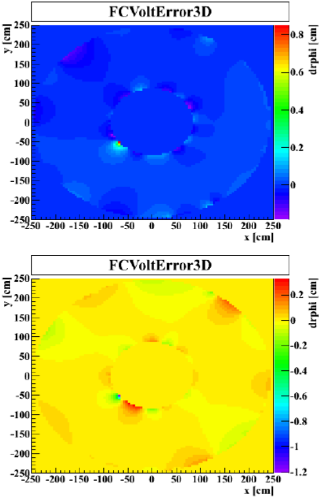

Figure 10 Resulting $r\phi$ distortions [6]

Shifted Rod and Strips

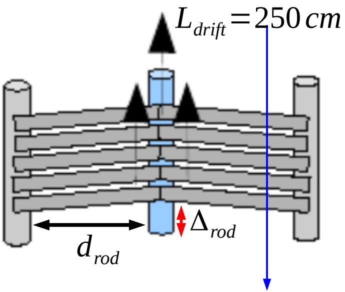

Figure 11 Shifted rod and strips scenario [6]

- 20° gap between rods

$\Rightarrow \frac{\Delta_{\mathrm{rod}}}{d_{\mathrm{rod}}} \cdot L_{\mathrm{drift}} \approx 8.3\Delta_{\mathrm{rod}}$

- Δ_{rod} $\mathcal{O}$ 100 µm → $\mathcal{O}$1 mm distortions

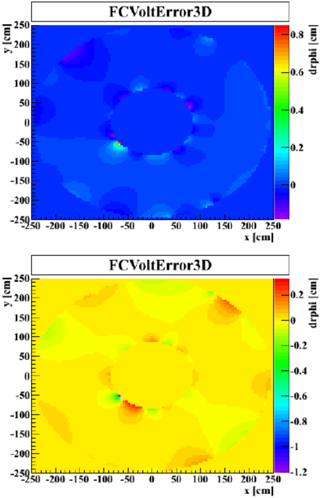

Figure 12 Resulting $r\phi$ distortions [6]

B Field Inhomogenities

- Axis of the magnet slightly shifted from centre

$\Rightarrow$ Causing B field inhomogenities in active volume

- $B_r \neq 0$
- $\frac{B_r}{B_z} \sim r$
- $\frac{B_r}{B_z} \approx 1\%,\ \omega\tau = 0.3$ at $r^* = 120 - 150$ cm
- $1\% \cdot 0.3 \cdot 250\,\text{cm} \approx \mathcal{O}\ 0.75\,\text{cm}$

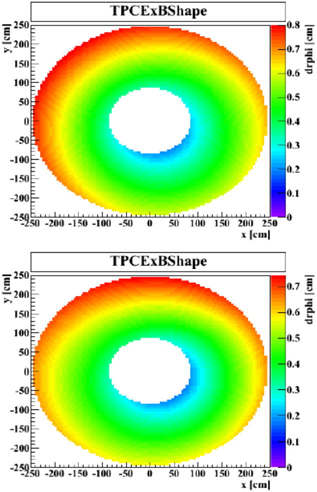

Figure 13 $r\phi$ distortions due to mag. field inhomogenities [6]

$E \times B$ Twist

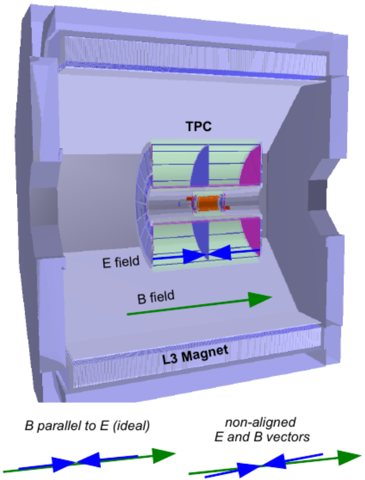

Figure 14 Sketch of $\vec{E} \times \vec{B}$ for ALICE[5]

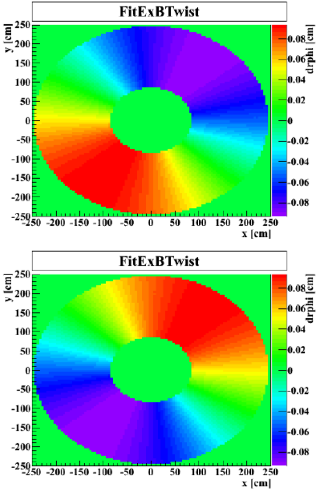

Figure 15 $dr\phi$ due to $\vec{E} \times \vec{B}$ effects.
$\mathcal{O}$ 1 mrad $\cdot\, \omega\tau \,\cdot$ 250 cm $\rightarrow \mathcal{O}$ 0.75 cm [6]

Calibration (RUN1)

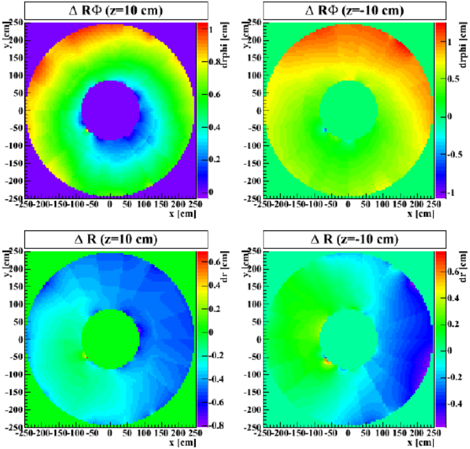

Figure 16 Composed correction maps for RUN1 based on physical models [6]

Assumptions:

- Distortions commute
- $\Delta = \sum_i k_i E_i$
- Distortions stable in time

BUT:

- Not directly observable

⇒ Set of unbiased observables O

- detector matching
- invariant masses
- cosmics
- $\sum_i k_i O_{E_i}$

RUN2

2015 – 2018

- Interaction rate: $\mathcal{O}$ 10 kHz (Pb-Pb)
- MWPC readout

Observations for RUN2

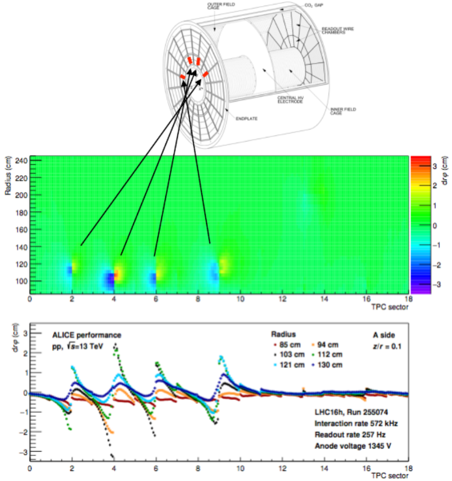

Figure 17 *drϕ* distortion hot spots at IROC boundaries [7]

- First high luminosity data of RUN2
- Large distortions up to $\pm 2.5\,\mathrm{cm}$
- Distortion well localised at sector boundaries

Expectations for Ar-CO2 (RUN2)

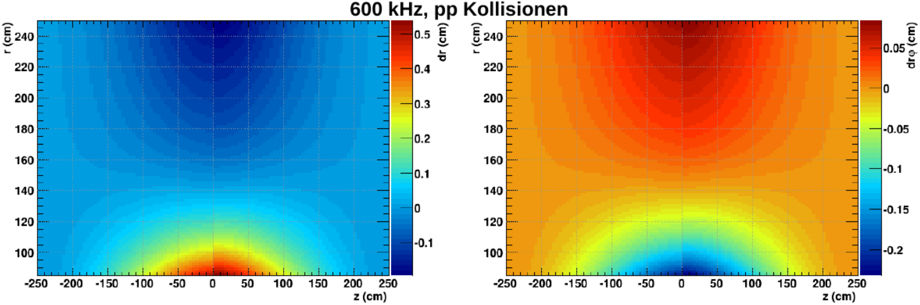

Figure 18 Expected drift field distortions for RUN2. *dr* (left), $dr\phi$ (right). Distortions smaller 1mm in most parts of the volume [2]

Highest track density in the middle for small radii:

dr up to 5 mm $dr\phi$ up to 2 mm

Space Charge Generation

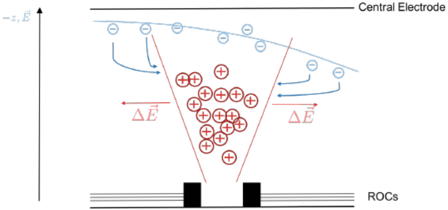

Figure 19 Sketch of space charge generation. $\mu_{\mathrm{ion}}/\mu_{\mathrm{e}} \approx 1000$ [3]

Sources:

- Backflow from gas amplification in ROCs
- Primary ionisation

$\Rightarrow$ RUN2:
Higher space charge accumulation
$\rightarrow$ higher distortions

- Mobility $\mu = \frac{v_{\mathrm{drift}}}{E}$
- $\mu_{\mathrm{NeCO2N2}}/\mu_{\mathrm{ArCO2}} \approx 2$
- Prim. ionisation:

RUN1	RUN2
$13\,\mathrm{cm}^{-1}$	$26\,\mathrm{cm}^{-1}$

- Higher luminosity in RUN2
- $\frac{\mathrm{flux}}{\mu} \cdot \frac{dE}{dx} \cdot T_{\mathrm{source}} \sim \rho_{\mathrm{ion}} \sim \Delta$

Measurement of Distortions (RUN2)

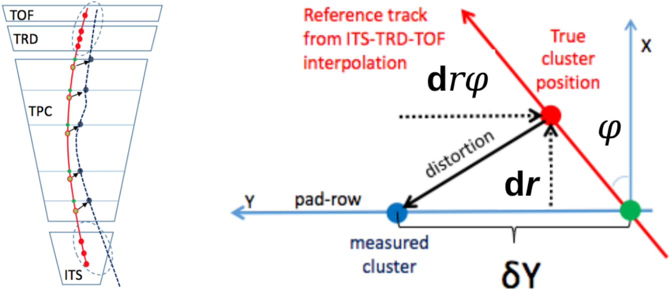

Figure 20 Sketch of distortion measurement in RUN2 via reference detectors ITS, TRD (now operational), TOF [2]

Distortion vector:

$(dr, dr\phi, dz)$

$\delta Y = dr\phi + dr \cdot \tan(\phi)$ ϕ : local inclination

$\delta Z = dz + dr \cdot \tan(\lambda)$ λ : dip angle

Observations for RUN2

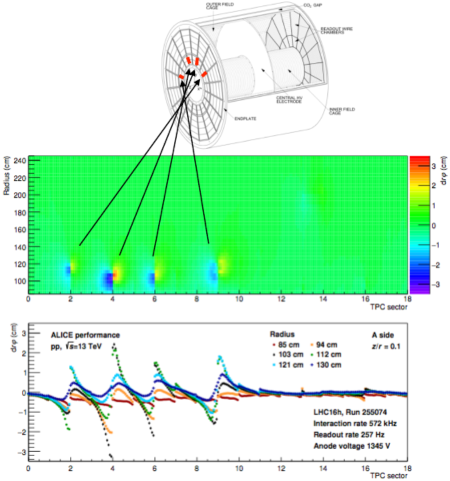

Figure 21 $dr\phi$ distortion hot spots at IROC boundaries [7]

- First high luminosity data of RUN2
- Large distortions up to $\pm 2.5\,\mathrm{cm}$
- Distortion well localised at sector boundaries

$\Rightarrow$ Source?

Dependence on the Drift Length

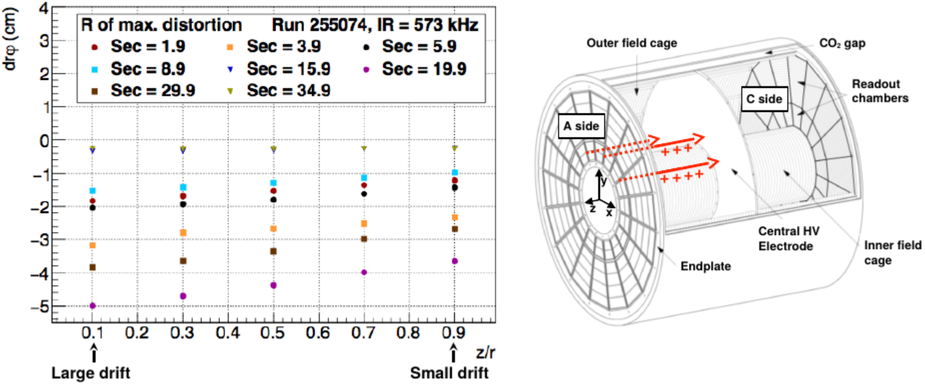

Figure 22 Drift length dependance of the distortions [7]

Linear dependence discovered

⇒ Columns of positive charge drifting from ROCs to CE

Origin of Space Charge

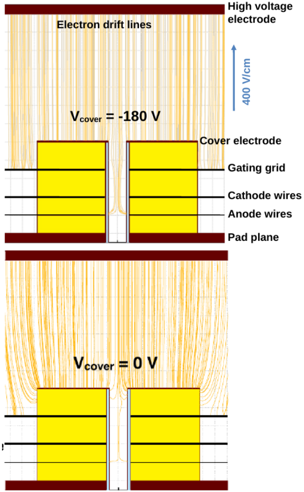

Figure 23 *E* field simulation at sector boundary by M. Ivanov [2]

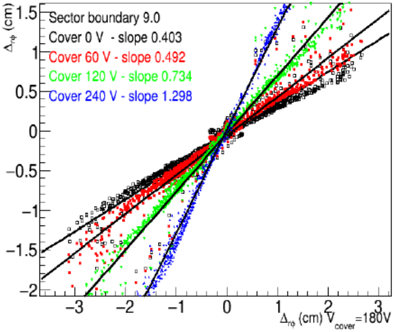

Figure 24 Cover voltage dependence of the distortions [7]

⇒ First indication that distortion originates between sectors

Inside or Outside Gap?

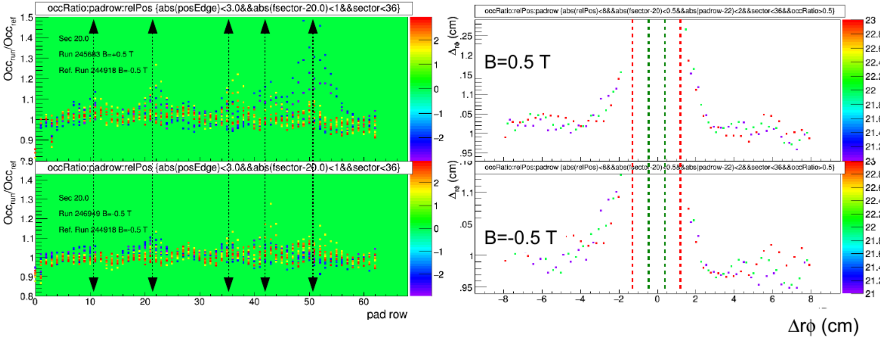

Figure 25 Occupancy studies to determine location of space charge source [7]

- Increase of occupancy close to distortion hotspots

⇒ Measure derivative of distortion with sub-pad granularity

⇒ Centre clearly inside the sector gap

Analitical Fit Model I

- E field of infinite line charge with uniform density λ
- $E(\Delta_r) = \frac{\lambda}{2\pi\epsilon_0\Delta_r}$

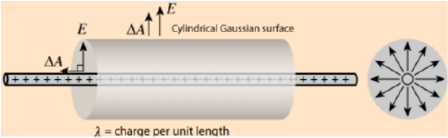

Figure 26 Scheme of Gauss' Law for infinite line charge [7]

$$E(r, r\phi) = \sum_{i=0}^{N} \frac{\lambda_i}{\sqrt{(r - R_i)^2 + (r\phi - R\Phi_i)^2}} \tag{5}$$

Analitical Fit Model II

$$E_r(r, r\phi) = \sum_{i=0}^{N} \frac{(r - R_i)\lambda_i}{(r - R_i)^2 + (r\phi - R\Phi_i)^2 + \Delta O_i^2} \tag{6}$$

$$E_{r\phi}(r, r\phi) = \sum_{i=0}^{N} \frac{(r\phi - R\Phi_i)\lambda_i}{(r - R_i)^2 + (r\phi - R\Phi_i)^2 + \Delta O_i^2} \tag{7}$$

$$dr = \frac{L_{\mathrm{drift}}}{E_z}(E_r - \omega\tau E_{r\phi}) \tag{8}$$

$$dr\phi = \frac{L_{\mathrm{drift}}}{E_z}(E_{r\phi} - \omega\tau E_r) \tag{9}$$

ΔO: finite radius size parameter (0.1 cm)
L_{drift}: drift length

Individual Fit Sector 9

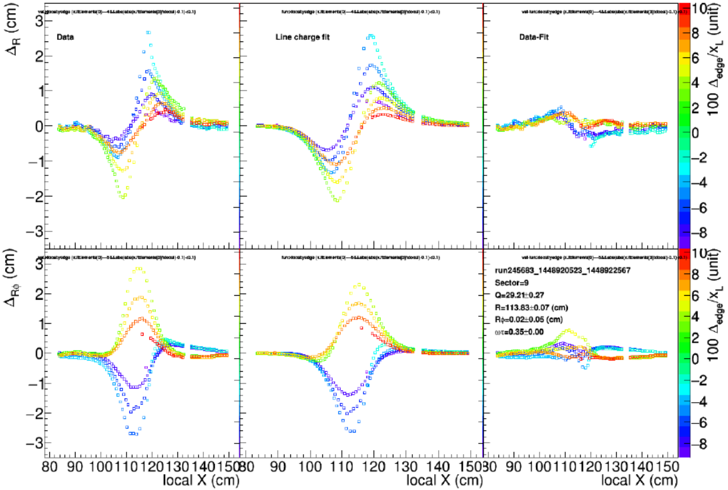

Figure 27 Line charge fit results for ΔR (top) and $\Delta R\Phi$ (bottom); sector 9. Data (left), Fit (middle), Data - Fit (right) [7]

Individual Fit Sector 6

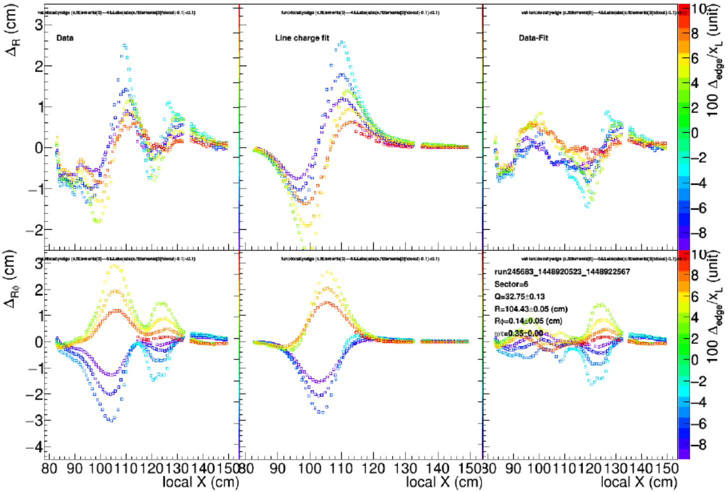

Figure 28 Line charge fit results for ΔR (top) and $\Delta R\Phi$ (bottom); sector 6. Data (left), Fit (middle), Data - Fit (right) [7]

Fits of Distortion Location

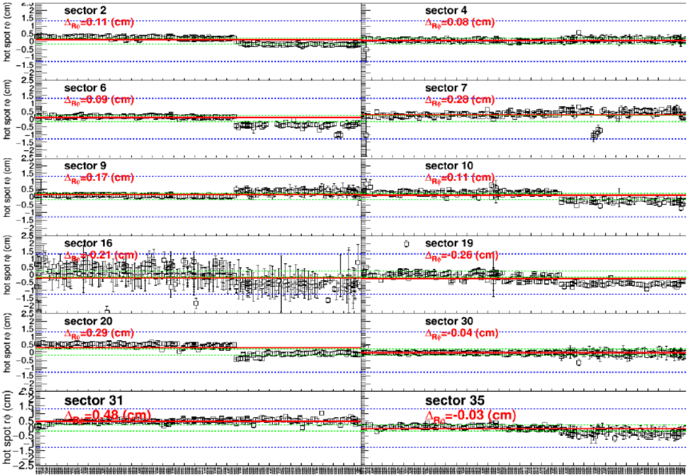

Figure 29 Results of position fitting of space charge in $r\phi$ for different sectors over 1 month Pb-Pb data. 0 cm $\hat{=}$ gap [7]

RUN3

starting 2021

- Interaction rate: $\mathcal{O}$ 50 kHz (Pb-Pb)
- GEM readout

GEM TPC Upgrade

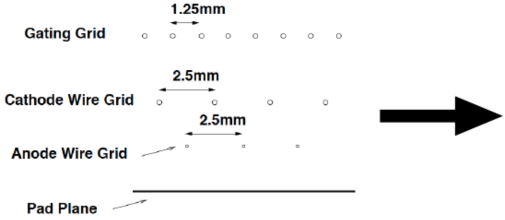

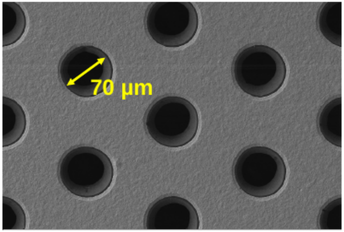

Figure 30 Schematic of the TPC upgrade. MWPC are replaced by GEM stacks. $\epsilon \approx 0 \to \epsilon = 20$ [2]

- Large ion backflow (IBF) expected

  $$\epsilon = 20 \frac{\text{ions}}{\text{prim. } e^-}$$

- $\rho_{sc} = N_{ion}(1 + \epsilon)$

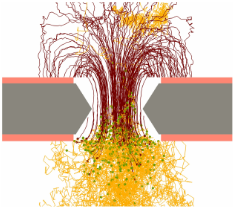

Figure 31 Simulation of ion backflow in a GEM [2]

Expected Distortions in RUN3

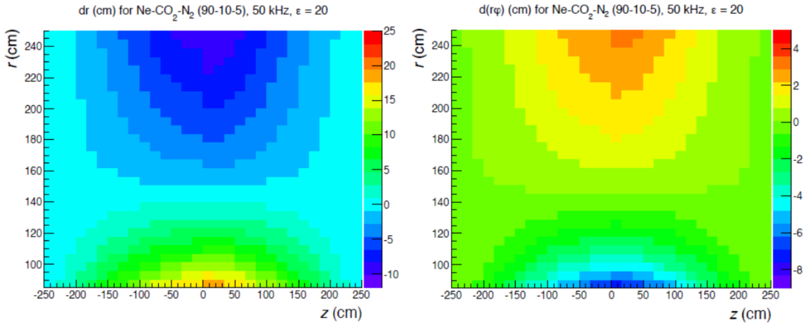

Figure 32 Expected distortions in r- and $r\phi$-direction [8]

Pb-Pb, 50 kHz, $\epsilon = 20$ (pp factor 5 less) :

- dr up to $\approx 20\,\text{cm}$
- $dr\phi$ up to $\approx 8\,\text{cm}$

$\Rightarrow$ Final calibration to $\mathcal{O}10^{-3}$ (200 - 500 µm)

Space Charge Map (RUN3)

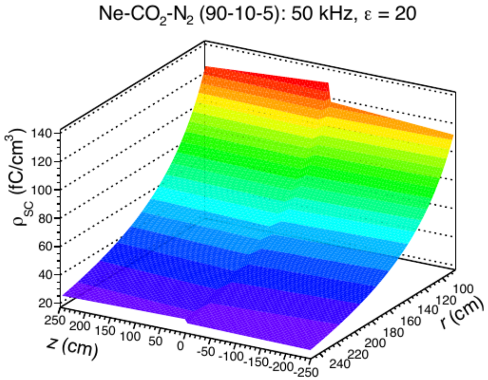

Figure 33 Fitted average space charge density for RUN3. Step due to background from muon absorber at C-side [9]

- Parametrised charged particle density distributions
- Plus symmetry assumptions

$\Rightarrow \rho_{sc}(r, z) = \frac{a - bz + c\epsilon}{r^d}$

- $1.5 < d < 2$

Distortion Calculation

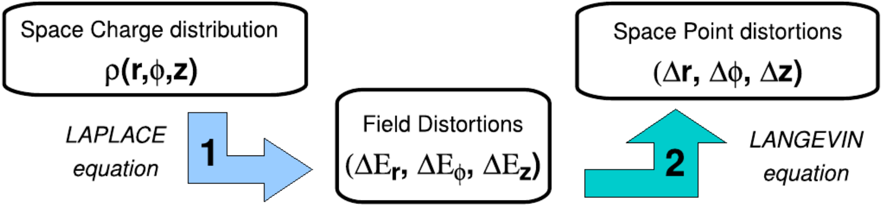

Figure 34 Basic principles of calculating the space point distortions [10]

Space Charge Density Maps

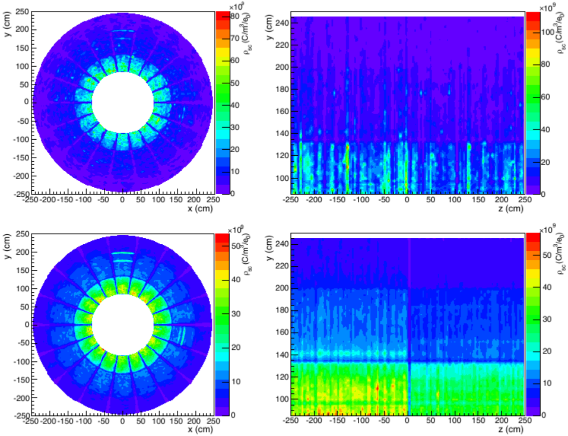

Figure 35 Space charge density maps for different pileup scenarios. 8000 (top), 160 000 (bottom). [9]

$\Rightarrow t_{\text{drift}} \approx 160\,\text{ms} \;\rightarrow$ pileup of 8000 events

Distortion Maps

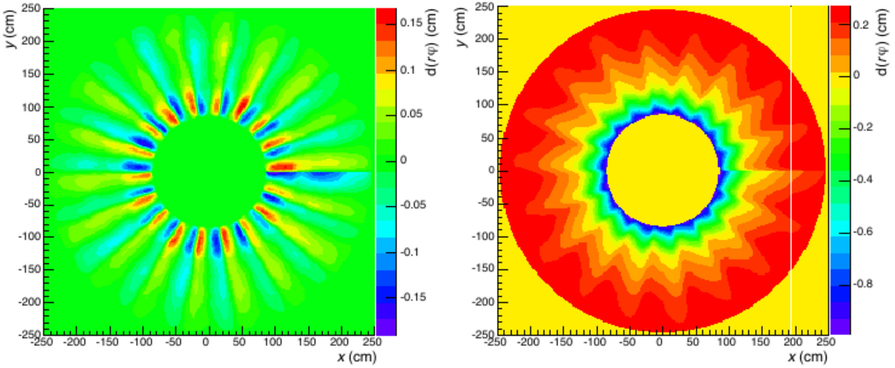

Figure 36 Projection of $r\phi$ distortion maps close to CE ($z \approx 10\,\text{cm}$) from 3D space charge map normalised to $\epsilon = 5$. $B = 0\,\text{T}$ (left) and $B = 0.5\,\text{T}$ (right) causing $E \times B$ effects [9]

Contributions to Space Charge Fluctuation

Pb-Pb, 50 kHz, $\epsilon = 20$:

- dr up to ≈ 20 cm
- $dr\phi$ up to ≈ 8 cm

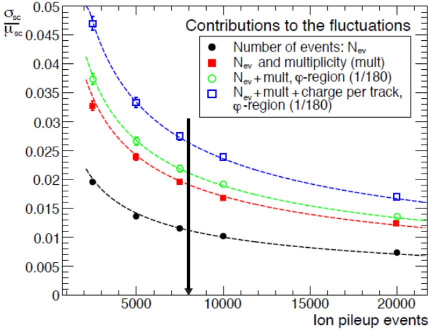

Figure 37 Different contributions to space charge fluctuation [8]

- Space charge fluctuations $\approx 3\%$
- Dominated by event and multiplicity fluctuations
- Knowing ρ_{av}:

  Max. ± 6 mm residual dist. in r

  Max. ± 2.5 mm residual dist. in $r\phi$

$\Rightarrow$ Sets constraints on update interval of ρ_{av}

Fluctuation Impact

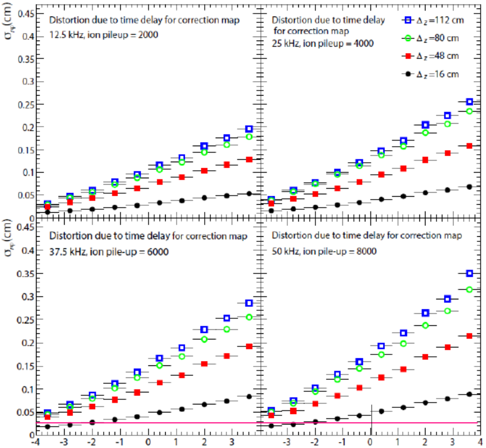

Figure 38 Estimate for update interval by shifting the SC map in *z*-direction [8]

- Already shift by 16 cm $\hat{=}$ 10 ms is significant

$\Rightarrow$ Required update time: $\approx$ 5 ms

- Instead: Δ_{ref} correction + residuals (pad current measurement)

$$\vec{\Delta} = \vec{\Delta}_{\text{ref}} \sum_i \frac{\partial \vec{\Delta}_{\text{ref}}}{\partial \rho^i_{\text{sc}}} \delta \rho^i_{\text{sc}}$$

Conclusion/Outlook

- Static distortions well understood
- Observations made during RUN2 well described by analytical model of line charges
- For RUN3 still some work to do, but on a good way

Backup

Dependence on Interaction Rate (RUN2)

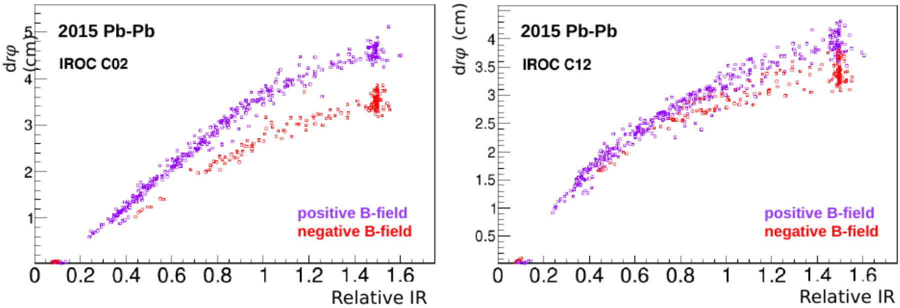

Figure 39 Saturation of distortion towards high interaction rate [2]

⇒ Primary e^- are deflected such, that they wont reach regions where they cannot create further space charge

Flux Dependance of Distortions

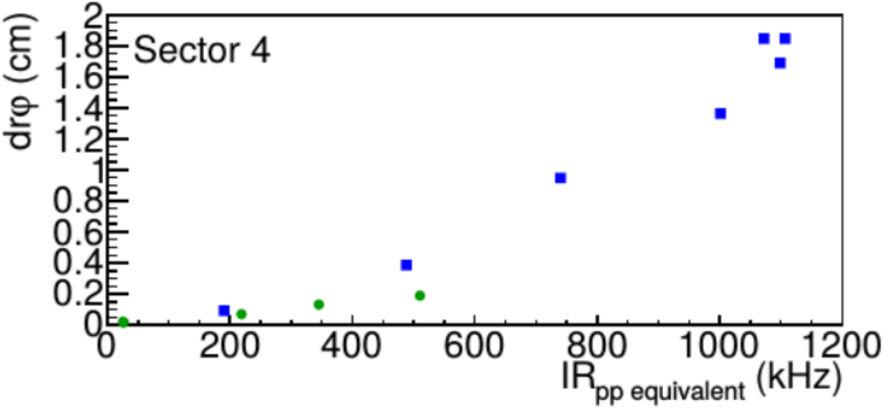

Figure 40 Exponential dependance of distortions from flux. 2017, pp, Ne-CO2-N2 (blue), 2013, pPb, Ne-CO2 [3]

Occupancy Approach

$$\frac{N_{cl}(V_{Drift}=400V/cm)}{N_{cl}(V_{Drift}=0V/cm)} = T_{el}\frac{L_{drift}}{L_{MWPC}} \approx O(200)$$

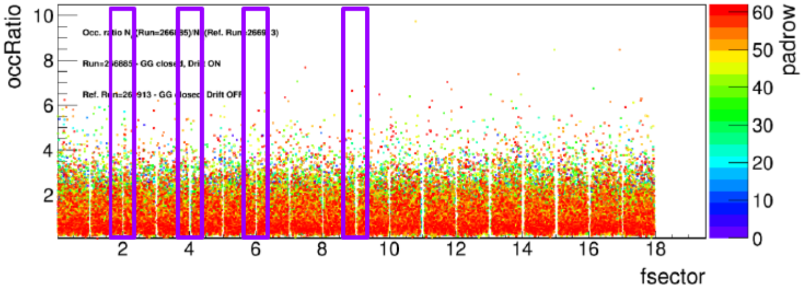

Figure 41 Cluster occupancy ratio with closed gating grid (GG) of different sectors [7]

- GG is 100% transparent → Occ. ratio $\mathcal{O}$ 200

⇒ No increased occupancy at gaps observed

CE Approach

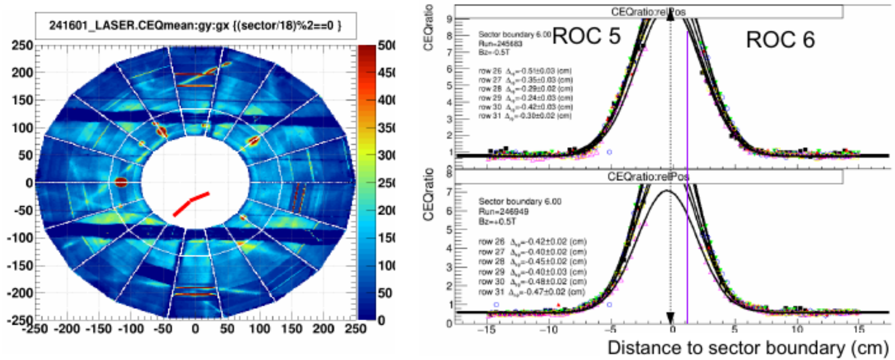

Figure 42 Laser scan of Central Electrode (CE) [7]

- Isotropic laser ligt to liberate e^{-} from CE
- Ions depositted on CE decrease its work function

$\Rightarrow$ Centre of gravity at sector boundaries

Individual Fit Sector 9

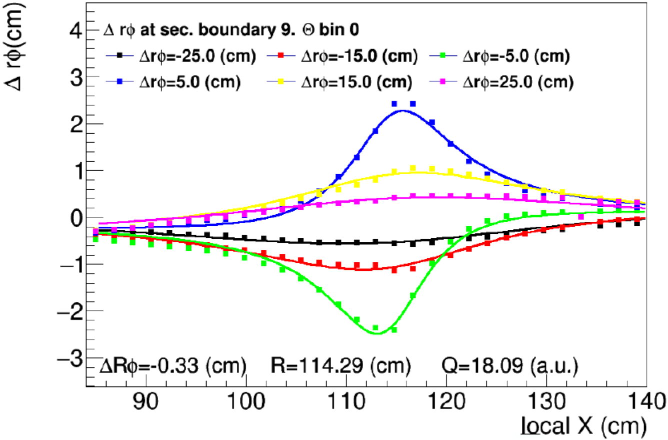

Figure 43 Results for sector 9. Lines are simulation results, no fit [7]

Position Fits for *R*-position

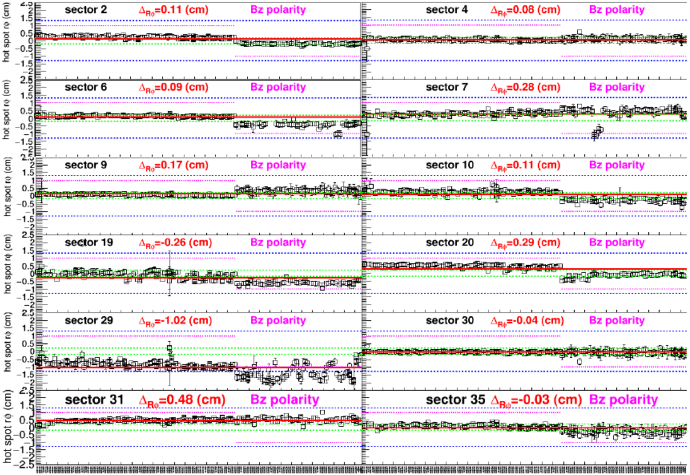

Figure 44 *R*-position fits. Segment 29 shows different behaviour [7]

Luminosity Dependence of Space Chage Density

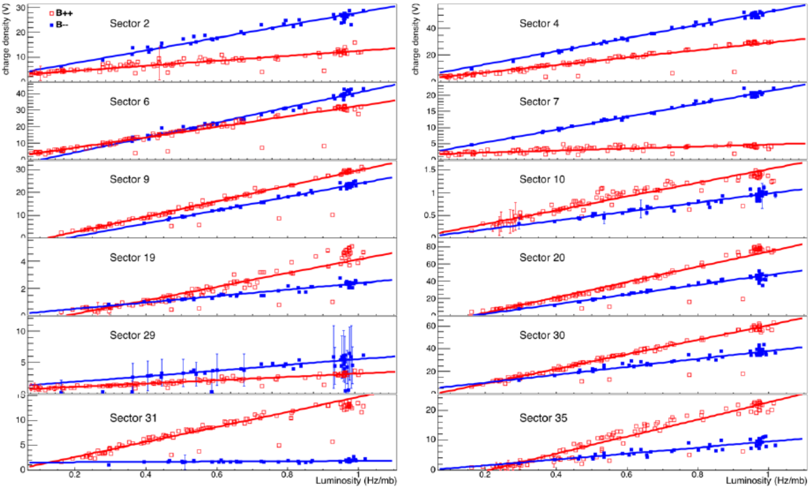

Figure 45 Linear dependence of space charge from luminosity for different B field orentation and sectors [2]

Expected Z Distortions in RUN3

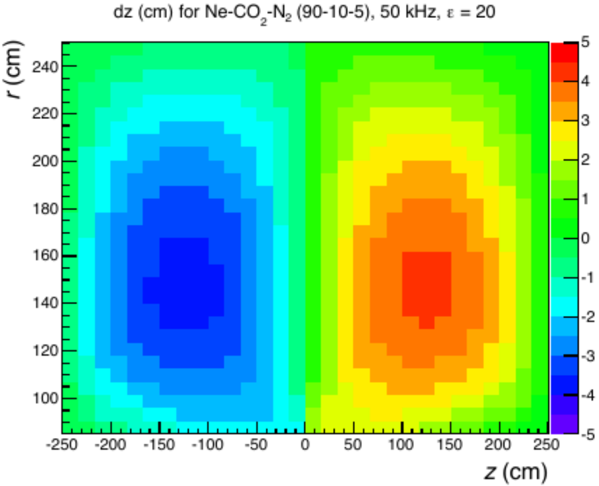

Figure 46 Expected distortions for RUN3 in *z*-direction [9]

Radial Dependence of Distortions

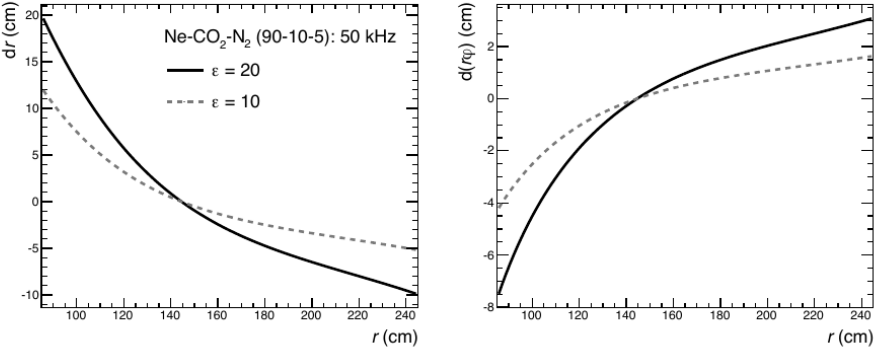

Figure 47 Radial Dependence of *dr* (left) and $dr\phi$ (right) near the central electrode ($z \approx 0$ cm) for $\epsilon = 20$ (solid) and $\epsilon = 10$ (dashed) [9]

ϵ Dependence of Distortions

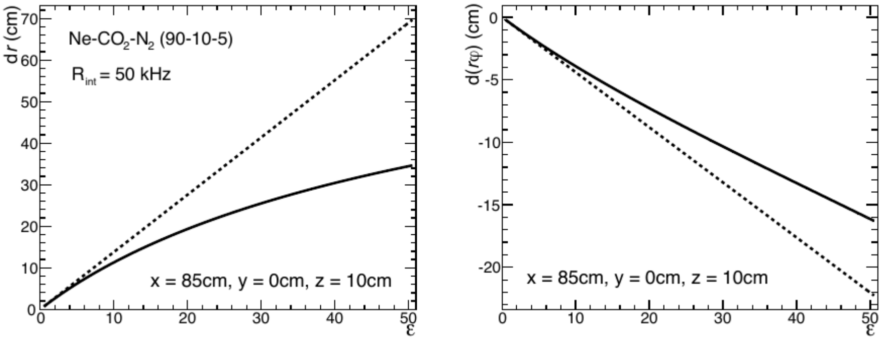

Figure 48 ϵ dependence of dr (left) and $dr\phi$ (right) near the CE ($z \approx 10\,\text{cm}$) and in the middle of a ROC ($y = 0$).
Dashed line indicates linear dependance (eye guide) [9]

Distortion Fluctuation Model

$$\frac{\rho_{\text{sc}}}{\mu_{\text{sc}}} = \frac{1}{\sqrt{N^{\text{ion}}_{\text{pileup}}}} \sqrt{1 + \left(\frac{\sigma_{\text{N}_\text{mult}}}{\mu_{\text{N}_\text{mult}}}\right)^2 + \frac{1}{F\mu_{\text{N}_\text{mult}}}\left(1 + \left(\frac{\sigma_{\text{Q}_\text{track}}}{\mu_{\text{Q}_\text{track}}}\right)^2\right)} \quad (10)$$

$\frac{1}{\sqrt{N^{\text{ion}}_{\text{pileup}}}} \approx 1.1\%$ fluctuation of number of pileup events

$\frac{\sigma_{\text{N}_\text{mult}}}{\mu_{\text{N}_\text{mult}}} \approx 1.4\%$ RMS of multiplicity distribution

$\frac{\sigma_{\text{Q}_\text{track}}}{\mu_{\text{Q}_\text{track}}} \approx 1.7\%$ relative variation of ionisation of single track

F: geometrical factor decribing relevant regions for space chage

References I

- Marian Ivanov.
  Personal communication.
- Ernst Hellbär.
  Raumladungsverzerrungen in der ALICE TPC.
  IKF Seminar, 14. Dezember 2017.
- Marian Ivanov.
  TPC and TRD flux and space charge distortion. Distortion model.
  ALICE TPC weekly meeting, 29th November 2017.
- Yannik Vetter.
  Space-Point Distortions.
  Seminar Report, Universität Heidelberg, 16th December 2016.

References II

J. Thomas M. Mager, S. Rossegger.

Composed correction framework for modeling the TPC field distortions in AliRoot.

ALICE Internal Note: ALICE-INT-2010-018 version 1.0, 2010.

Marian Ivanov.

TPC space point distortion and calibration. Pass 0 and PassX calibration.

ALICE offline week, 10th March 2011.

Marian Ivanov.

Locating the origin of space charge distortions. Analytical models.

ALICE Technical Board Meeting, 6th April 2017.

References III

Jens Wiechula.
TPC run 3 O2 discussion.
TPC micro workshop on Continuous readout (simulations), 8th October 2014.

The ALICE collaboration.
Upgrade of the ALICE Time Projection Chamber.
Technical Report CERN-LHCC-2013-020. ALICE-TDR-016, Oct 2013.

J. Thomas S. Rossegger.
Space-charge effects in the ALICE TPC: a comparison between expected ALICE performance and current results from the STAR TPC.
ALICE Internal Note: ALICE-INT-2010-017 version 1.0, 2010.

References IV

Ernst Hellbär.
Ion Movement and Space-Charge Distortions in the ALICE TPC.
mathesis, Institut für Kernphysik Goethe-Universität, Frankfurt am Main, 2015.

Ernst Hellbär.
Space-charge distortions in der ALICE TPC.
Presentation Slides.

Marian Ivanov.
Where do we stand with respect to TDR performance.
TPC planning meeting, 2nd February 2011.